2004 FALL MEETING PROCEEDINGS

Symposium OO
Materials Issues in Art and Archaeology VII

Editors: P. Vandiver, J. Mass, A. Murray

MRS Proceedings Volume 852
Purchase this Volume: Order Online | Download Order Form

Confocal X-ray Fluorescence (XRF) Microscopy: A New Technique for the Nondestructive Compositional Depth Profiling of Paintings

Arthur R. Woll[1], Donald H. Bilderback[1,2], Sol Gruner[1,3], Ning Gao[4], Rong Huang[5], Christina Bisulca[6] and Jennifer Mass[6,7]
[1]Cornell High Energy Synchrotron Source, Cornell University, Ithaca, NY 14853, U.S.A.
[2]School of Applied & Engineering Physics, Cornell University, Ithaca, NY 14853, U.S.A.
[3]Dept. of Physics, Cornell University, Ithaca, NY 14853, U.S.A.
[4]X-ray Optical Systems, Albany, NY, 12203, U.S.A.
[5]Advanced Photon Source, Argonne National Laboratory, Argonne, IL 60439, U.S.A.
[6]University of Delaware, Newark, DE, 19716, U.S.A.
[7]Winterthur Museum, Winterthur, DE 19735, U.S.A.

ABSTRACT

A confocal x-ray fluorescence microscope was built at the Cornell High Energy Synchrotron Source (CHESS) to determine the composition of buried paint layers that range from 10-80 μm thick in paintings. The microscope consists of a borosilicate monocapillary optic to focus the incident beam and a borosilicate polycapillary lens to collect the fluorescent x-rays. The overlap of the two focal regions is several tens of microns in extent, and defines the active, or confocal, volume of the microscope. The capabilities of the technique were tested using acrylic paint films with distinct layers brushed onto glass slides and a twentieth century oil painting on canvas. The position and thickness of individual layers were extracted from their fluorescence profiles by fitting to a simple, semi-empirical model.

INTRODUCTION

Information about paint layers below the presentation surface in a painting can be used to address questions regarding the work's authenticity, the extent of previous restorations, the working methods of the artist, and the piece's condition [1,2,3]. The most common technique for characterizing layered paint structures in works of art is scanning electron microscopy-energy dispersive spectroscopy (SEM-EDS) [1,4,5] This technique requires that a sample be taken and studied in a prepared cross-section, however, and typically the areas of greatest interest (such as the subject of a portrait) are those areas that are least available for sampling. For over 30 years, nondestructive characterization of buried paint layers has been carried out by neutron autoradiography (NA) [2]. While valuable, NA nevertheless reveals only the presence of certain elements, not their relative positions, and the technique requires the irradiation of the painting.

Recently, researchers have attempted to extend the use of traditional, non-destructive characterization tools such as x-ray fluorescence (XRF) [4,5,6,7] and proton-induced x-ray emission (PIXE) [3,8,9] to address the problem of compositional depth profiling of paintings. One XRF method consists of deducing the relative positions of paint layers by monitoring changes in the ratios of the Kα and Kβ x-ray intensities that result from the selective absorption of one of the paint layer's fluorescence lines [6,7]. This phenomenon will occur when the absorption edge of the pigment in the upper paint layer falls between the two x-ray lines of the pigment in the buried layer. This method cannot be applied to all possible paint layer combinations, however. Another method involves increasing the proton beam energy during a PIXE analysis to increase the spectral contribution of the pigments in the lower paint

layers. This technique has promise but has not been successfully applied beyond three paint layers [8]. A third method involves progressively decreasing the incident angle of the proton beam in a PIXE experiment to increase the contribution of the topmost paint layer to the resulting x-ray spectrum. This method has proven unreliable for paint layer thicknesses of less than or about 10 μm [3].

During the past two years, improvements to x-ray optics based on hollow glass capillary tubes [10] have enabled a different approach to achieving depth-resolved XRF. The approach, called confocal XRF, is illustrated in Figure 1. One optic focuses the incident beam, while the other, placed perpendicularly to the first, gathers fluorescence only from the region of the sample where the focal cone of the second optic intersects that of the first. To obtain the composition as a function of depth, the sample is raised through this confocal volume.

Among the first experiments demonstrating this technique were those performed by Proost et al. at HASYLAB [11] on thin, buried metal films. Kanngiesser et al. have made use of confocal XRF to characterize paint layers of two Indian Mughal miniatures [12]. In this experiment, the leading edges of the fluorescence vs. depth curves were used to measure the relative positions of different layers. While valid for the samples in Ref. 12, this approach is insufficient for more complex layered structures. Also, this approach will not work if a low-Z (undetectable) pigment layer, such as an organic lake, is present between two high-Z pigment layers. Ideally, one desires a robust, general technique of extracting layer positions and thicknesses from fluorescence vs. depth curves. One could then raster scan a painting, determining the compositional depth profile at each raster point (a single depth scan takes 1-2 min.). Combining these scans would allow for the examination of virtual cross-sections from any region of a painting, and for paint layer compositions and thicknesses to be obtained in a totally nondestructive manner.

To evaluate the capabilities and limitations of this technique for obtaining depth-dependent compositional information from layered paint structures, a confocal x-ray fluorescence microscope was constructed at CHESS. In this article, we discuss depth-profile measurements of several multilayered acrylic paint samples on glass slides in addition to a twentieth century oil painting on canvas. Specifically, we illustrate how to take the measured depth resolution of the microscope into account, generalizing the scope of this technique to include thickly layered samples where absorption must be included in layer thickness calculations. While synchrotron radiation was used to perform these initial evaluations of the technique, confocal measurements of lower resolution can be obtained on a suitably modified stand-alone XRF system [13].

EXPERIMENTAL DETAILS

Microscope design

The confocal XRF experiments were carried out at CHESS station D1, using monochromatic radiation at 16 keV, selected using a 1% bandpass multilayer monochromator with a d-spacing of 25.5 angstroms. The unfocussed flux at the sample was approximately $6x10^{11}$ photons/sec/mm^2. A single-bounce monocapillary (#Pb605), developed at CHESS [14], was used to provide a focused incident beam of approximately 20 μm in diameter, while a double-focusing polycapillary lens [11,15] with an input acceptance angle of 15.4º [9,13], on loan from X-ray Optical Systems [16] was used to collect x-ray fluorescence from the sample. For depth-profiling, the sample is scanned normal to its surface oriented 45^o to the incident beam. The depth resolution is determined by the projection of the confocal volume onto this scanning direction.

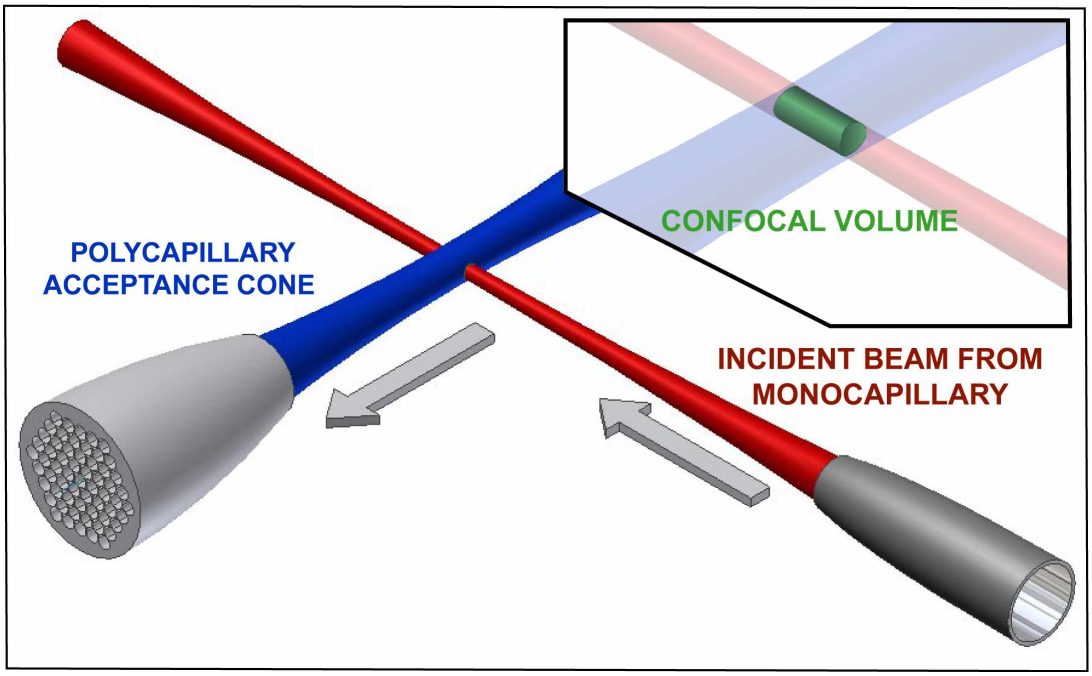

Figure 1. Geometry of the confocal XRF microscope. The incident beam is focused by a monocapillary lens to approximately 20 μm in diameter. Fluorescence is collected by a polycapillary, with a minimum collection area of 20-60 μm^2, depending on fluorescence energy. The intersection between the two defines the confocal volume. Samples are scanned through this confocal volume at 45º to both beams.

For alignment and scanning purposes, the monocapillary, sample, and polycapillary were all mounted to motorized translation stages. Fluorescence was collected by a Rontec Xflash silicon drift chamber placed behind the polycapillary. This detector has an energy resolution of approximately 0.16 keV. For clarity, the energies of particular fluorescence signals are given to a precision of 0.1 keV when their source is unclear (e.g. Ba Lα vs. Ti Kα), but to 0.01 keV when unambiguously identified with particular elemental lines. Data described below were taken with a 0.062" aluminum attenuator in the incident beam, both to reduce the fluorescence signal at the detector and to avoid potential radiation damage to the paint layers.

Sample preparation

Ten different pigments were obtained from Kremer Pigments: blanc fixe ($BaSO_4$), lead white $2Pb(CO_3)Pb(OH)_2$, titanium white (TiO_2), chalk ($CaCO_3$), malachite ($Cu_2CO_3OH_2$), iron oxide yellow (Fe_2O_3), orpiment (As_2S_3), cadmium yellow (CdS), chromium oxide green (Cr_2O_3), and vermilion (HgS). Paints were prepared from each of these pigments by mixing 1 ml of pigment with 4 ml of a 20% v/v mixture of copolymer binder, Paraloid B-72 [17] and acetone. Layered paint samples were prepared by brushing each paint onto the frosted end of a Fisher glass slide. Paint layers were allowed to dry for 15-20 minutes between each layer to minimize the mixing of layers at the interface. For paint chronology 2 a second sample was prepared with a poly(vinyl acetate) (PVAc) spacer layer applied between each paint layer. Table I lists paint layer chronologies for the test samples.

Table I Chronologies used in prepared paint samples, listed in order of application

Chronology 1	*Chronology 2*
Lead white	*Chalk*
Malachite	*Iron oxide*
Chrome green	*Orpiment*
Cadmium yellow	*Titanium white*

RESULTS

Characterization of the confocal volume

Figure 2 shows the results of depth scans of a variety of thin metal films deposited onto glass slides. The full-width at half maximum (FWHM) of each fluorescence peak is plotted as a function of fluorescence energy. The thickness of all films is nominally 500 nm, far smaller than the size of the confocal volume perpendicular to the surface. Thus the widths shown in Fig. 2 represent the projected size of the confocal volume normal to the surface as a function of energy. This energy-dependence results from that of the polycapillary, whose focal size varies from approximately 67 μm at 4.5 keV to 24 microns at 10.5 keV. The focal size of the monocapillary, on the other hand, has been previously measured to be 17-23 μm, independent of energy.

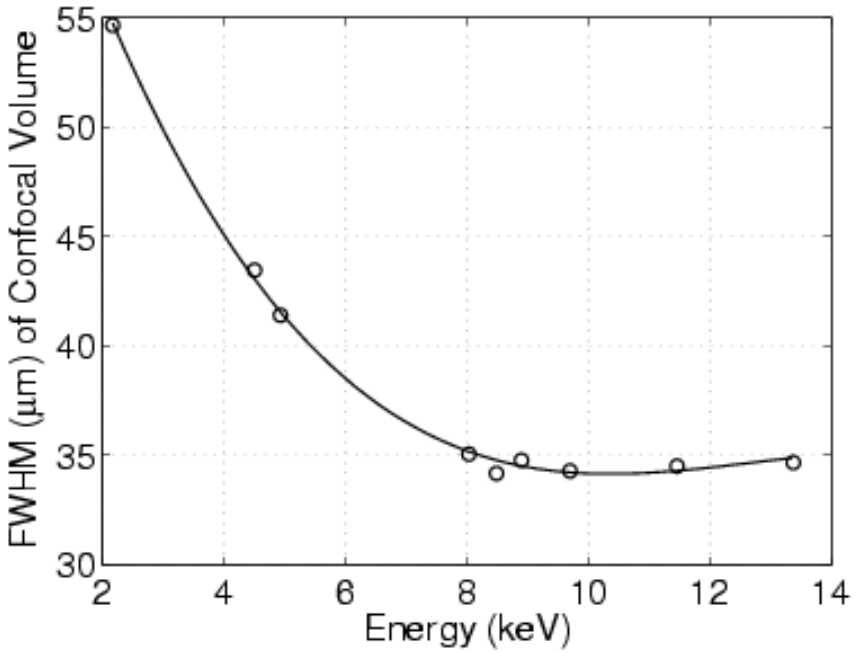

Figure 2. Full-width at half maximum (FWHM) of fluorescence intensity vs. depth from scans of thin (≈500 nm) titanium, copper, and gold films, plotted as a function of fluorescence energy. These values determine the energy-dependent resolution of the confocal XRF microscope. The solid line is a third order polynomial fit to the measured values.

In order to model depth scans from real paints, we require knowledge of this projected width at all fluorescence lines of interest. The solid line in Fig. 2 shows a third-order polynomial fit to the data. In the discussion of our fitting results below, we use this fit to generate a gaussian-resolution function at arbitrary photon energies. Models of elemental density as a function of depth are then convolved with this resolution, resulting in curves that can be directly compared to the measured profiles.

Layered paints on glass slides

Figure 3 shows a cross-section of a multilayered paint sample prepared with chronology 1 in Table I. Figure 4a shows the raw fluorescence vs. depth data obtained from scanning this sample through the confocal microscope. Fluorescence intensity is indicated by brightness on a logarithmic scale. The scan consists of 126 different fluorescence spectra, each with an integration (live) time of 1 second. The sample is translated normal to the surface by four microns between each spectrum. Depth and energy are represented on the x- and y- axes, respectively. The pigments in the buried paint layers are indicated by fluorescence peaks from their main inorganic constituent: cadmium (3.13 and 3.32 keV, $L\alpha_1$ and $L\beta_1$), chromium (5.42 and 5.95 keV, $K\alpha_1$ and $K\beta_1$) copper (8.05 and 8.91 keV, $K\alpha_1$ and $K\beta_1$), and lead (10.55, 12.61, and 14.76 keV, $L\alpha_1$, $L\beta_1$, and $L\gamma_1$) The four different layer depths are clearly indicated by the different peak locations on the x-axis.

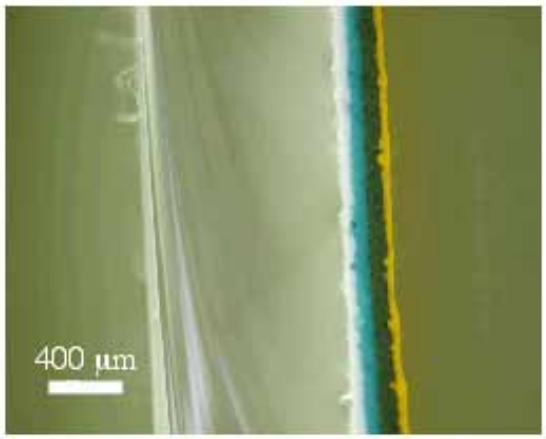

Figure 3. Optical cross-section of a multilayered paint sample on a glass slide prepared with chronology 1. The four pigments, from left to right, are lead white, malachite (Cu-based), chromium oxide green, and cadmium yellow.

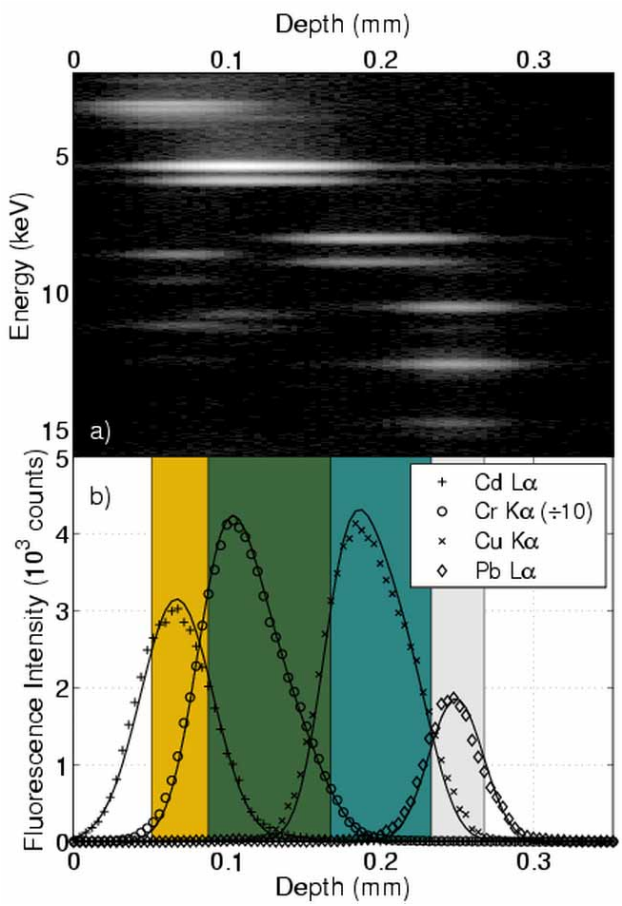

Figure 4. (a) Fluorescence spectra plotted as energy vs. depth for sample prepared with chronology 1 at 4-micron intervals. Brightness indicates intensity on a logarithmic scale. (b) Intensity vs. depth of several particular fluorescence peaks from (a). The Cr Kα data is rescaled for the plot, as indicated by the inset. The solid lines and shaded regions represent the best-fit curves and individual layer profiles as extracted from fits to the model described below.

Figure 4a also reveals the presence of a Zn-based filler that had been added to the cadmium yellow pigment ($K\alpha_1$ and $K\beta_1$ lines at 8.64 keV and 9.57 keV). Figure 4b shows the intensity of the Kα lines of each of the four elements identified in Fig. 4a. The peaks are clearly offset from one another, indicating the different layer depths. To accurately extract information about each layer in the sample, the data were fit to a four-parameter model of fluorescence vs. depth. The model consists of a density profile convolved with a resolution function whose width is determined by the data shown in Fig. 2 [18]. The four parameters are the locations of the top and bottom interfaces, an attenuation factor μ, (which accounts for the attenuation of both the incident and fluorescent x-rays), and a proportionality constant related to the layer density, microscope sensitivity, and incident flux.

The solid lines in Fig. 4b correspond to best-fit curves of each peak to this model. The best-fit density profiles for each element are represented by the shaded areas, and correspond to layer thicknesses of 38 (cadmium yellow), 80 (chromium oxide green), 69 (malachite), and 34 (lead white) microns. Cross-sections were measured to check the layer thicknesses as deduced from the fits. The region was chosen to be close to that examined by XRF, as determined by color centers on the glass

substrate (formed by the incident beam). As shown in Table II for chronology 1, the best-fit thicknesses from confocal XRF are in agreement with the thickness ranges measured optically.

Table II Measured Paint Layer Thickness - Chronology 1

Layer	Optical Thickness Measurement Range /Average (μm)	Confocal XRF (±5 μm)
Cadmium yellow	34-62 / 35	38
Chrome Green	62-90 / 86	80
Malachite	63-97 / 68	69
Lead white	35-62 / 48	34
- Glass slide -		

The results for the chronology 2 sample that contained a PVAc spacer layer between each paint layer provided the composition and approximate position of each paint layer (see Table III, raw data not shown). Note that only one of the PVAc spacer layers was detected, most likely due to the variable thicknesses of the brush-applied layers. Based on the resolution of the microscope, one can estimate that the remaining two spacer layers were under five microns thick.

Table III. Measured Paint Layer Thickness - Chronology 2

Layer	Optical Thickness Measurement: Range /Average (μm)	Confocal XRF (±5 μm)
Titanium White	13-33 / 22	29
Orpiment	10-36 / 17	10
PVAc	7-23 / 16	30
Iron oxide	20-43 / 29	8
Chalk	7-30 / 17	14
- Glass slide -		

While confocal XRF cannot reveal the composition of the PVAc organic layer, it does give its thickness and position by virtue of the positions of adjacent interfaces. The discrepancies observed between the confocal XRF-measured PVAc and iron oxide layer thicknesses and the optical microscopy measurements are most likely due to the variable thicknesses of these layers and the challenge of performing both types of measurements in precisely the same location.

20th Century oil on canvas

As a more realistic test of the utility of confocal XRF, we also examined a 20th c. oil painting on canvas [19]. Figure 5a shows the results of a single-depth scan from this painting. The data are heavily dominated by lead fluorescence. In addition to the Pb Lα, Lβ and Lγ lines, several weaker Pb lines are present, namely two M-lines at 2.40 and 3.12 keV and the Lι and Lη lines at 9.18 and 11.35 keV [20]. Additional lines at 5.90, 6.40, and 7.06 keV correspond to the Mn and Fe K lines, while those at 3.69 and 4.01 keV correspond to Ca $K\alpha_1$ and $K\beta_1$. The combination of Mn and Fe is associated with umber, a pigment used both by itself and, frequently, as a component of an underpainting or ground. Unlike Fig. 4, no clear evidence of layering is present. Rather, the calcium, umber, and lead signals all overlap,

suggesting that the pigments are mixed.

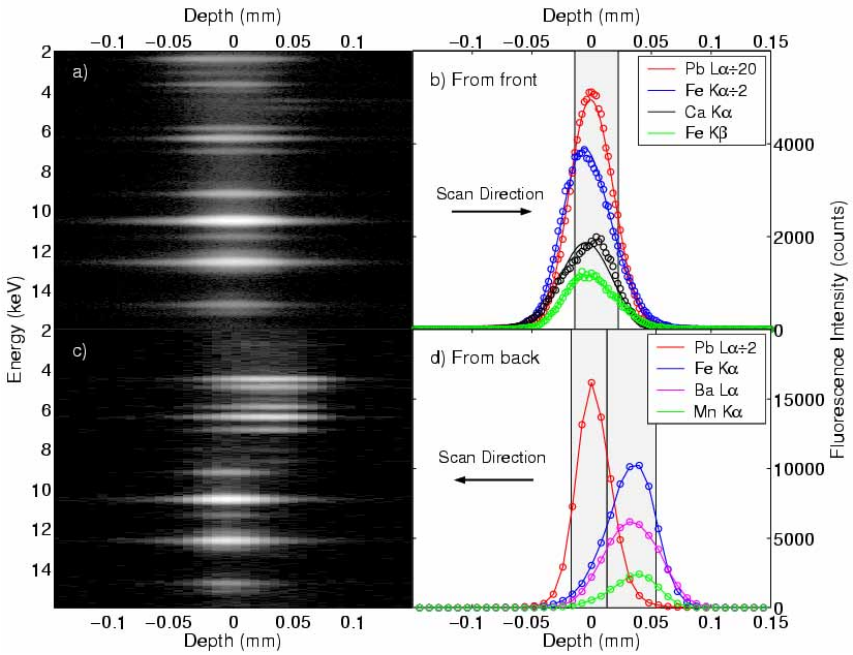

Figure 5 Fluorescence spectra as a function of depth obtained with the incident beam entering from the paint side (a, b) and canvas side (c, d) of a 20th c. oil painting. The top layer consists of lead, umber (iron and manganese) and calcium. The buried layer consists of titanium, barium and umber. In (a) and (c) spectra are separated in depth by 2 microns and 8 microns, respectively. Brightness indicates intensity on a logarithmic scale.

Figure 5b shows depth profiles of several of the fluorescence lines identified in Fig. 5a. Best-fit curves to the model of Eqs. 1-2 are also shown, in addition to the best-fit profile (gray region) of the lead fluorescence. The best-fit thicknesses of the lead and calcium lines were 36 and 31 microns, respectively, while that of the Mn and Fe lines was 51 microns. Furthermore, the best-fit position of the top interface of the lead, calcium, and umber lines was coincident to within 5 microns. Thus, we conclude that the paint layer represented by Fig.5a is a mixture of a calcium, lead, and umber-containing pigments, and is approximately 30-40 microns thick. The larger best-fit value for umber suggests that umber is a constiutent of an additional, buried layer.

While valuable, the information from Figs. 5a-b is incomplete. In particular, there may be other pigment layers between the uppermost lead-containing layer and the canvas. Apart from the larger best-fit thickness of the Mn and Fe lines, careful inspection of Fig. 5a shows weak peaks corresponding to 4.5 and 4.9 keV that originate beneath the lead layer. These energies correspond closely both to the principal K lines of titanium (4.51, 4.93 keV) and the principal L lines of barium (4.47 and 4.83 keV). Next, we scanned approximately the same location on the painting, within 2 mm of the first scan, but with the canvas side facing the incident beam. Figures 5c,d show the data obtained from this scan.

In Figs. 5c,d, two distinct layers are evident. The right-hand layer in the figure exhibits strong fluorescence at 4.5 and 4.9 keV, coincident with the weak lines in Fig. 5a, in addition to weaker lines at 5.1 and 5.5 keV. These energies correspond to weaker L-lines of Ba, namely Ba $L\beta_2$ and $L\gamma_1$, verifying the presence of barium. The best-fit thickness of this layer is 41 microns. This layer also exhibits Mn

and Fe lines similar to those shown in Fig. 5a. Fitting to these lines verifies that it fully overlaps the barium fluorescence. The left hand layer in Figs. 5b,d, closer to the painting surface, exhibits strong lead fluorescence and gives a best-fit thickness of 30 microns, close to the value of 36 microns obtained from the lead layer in Fig. 5b. We conclude that the lead peaks from Figs. 5b,d correspond to the same layer, and that the barium arises from a buried ground or underpainting layer. Note that no evidence of calcium appears in the lead-rich layer in this scan, indicating that the high-density barium layer completely absorbs the calcium fluorescence.

We tested our results for the 20th century oil painting using a cross-section analyzed by SEM on the same area of the sample used for confocal XRF. Overall, the SEM data strongly corroborate our findings. In particular, this area of the sample is made up of two layers, the top layer varying from 30 to 40 microns in thickness and the bottom layer approximately 40 microns thick. Lead and calcium are present only in the top layer, while umber is present in both layers. Barium and titanium are present in the ground layer only. In summary, we have demonstrated the successful reconstruction of the stratigraphy of the painting. In particular, we determined the composition, thickness and relative position of both principal layers in the painting for a particular region. Scanning from both directions allowed the identification of low energy fluorescence lines originating from buried layers that were strongly absorbed by lead and barium in the two layers.

CONCLUSIONS

Our results establish the feasibility of non-destructively obtaining detailed composition vs. depth information from multilayered paint structures using confocal XRF. We characterized test samples with up to five distinct layers and a complex two-layer structure in a twentieth century oil painting by M. Bockrath. The relative positions of these layers were obtained *directly* from the data. A more detailed, but straightforward, analysis was used to obtain additional information, such as the absolute layer position relative to the surface and the layer thicknesses. At least one lab-based, confocal XRF system that does not require a synchrotron x-ray source is being developed [13]. As such systems become more common, we expect that confocal XRF to become an invaluable research tool for conservation science in the characterization of multi-layered inorganic structures. Such detailed spatial information is not available through traditional nondestructive techniques such as XRF and PIXE.

ACKNOWLEDGEMENTS

This work is based upon research conducted at the Cornell High Energy Synchrotron Source (CHESS) which is supported by the National Science Foundation under award DMR 0225180 and the National Institutes of Health/National Institute of General Medical Sciences. The confocal microscope construction was supported by the National Science Foundation Instrumentation for Materials Research award DMR 0415838.

The authors would like to thank Mark Bockrath, Richard Wolbers, and Joyce Hill Stoner for their helpful suggestions and discussions, and Mark Bockrath for the donation of his painting.

REFERENCES

1. W. S. Taft and J.W. Mayer, *The Science of Paintings*, Springer-Verlag, New York (2000).
2. M. Ainsworth, J. Brealy, E. Haverkamp-Begemann, P. Meyers, et al. *Art and Autoradiography:*

Insights into the Genesis of Paintings by Rembrandt, Van Dyck, and Vermeer, The Metropolitan Museum of Art, New York (1982).
3. C. Neelmeijer, I. Brissaud, T. Calligaro, G. Demortier, A. Hautojarvi, M. Mader, L. Martinot, M. Schreiner, T. Tuurnala, and G. Weber, *X-ray Spectrometry*, **29**, 101 (2000).
4. K. Ashworth, Lignelli, T.A. and M. Butler, Postprints (American Institute for Conservation of Historic and Artistic Works. Paintings Specialty Group), 1-9, (1988).
5. J.H. Stoner, Schmiegel, K, and Carlson, J. H., *Preprints of Papers Presented at the Seventh Annual Meeting of the American Institute for Conservation of Historic and Artistic Works* (1979) 139-148.
6. M. Schreiner, M. Mantler, F. Weber, R. Ebner, and F. Mairinger, *Adv. X-ray Anal.*, **35**, 987 (1992).
7. C. Roldan, J. Coll, J.L. Ferrero, and D. Juanes, *X-ray Spectrometry*, **33**, 28 (2003).
8. Neelmeijer, C. and M. Mader, *Nucl. Instrum. & Meth. B,* **189**, 293, (2002).
9. A. Denker and J. Opitz-Coutureau, *Nucl. Instrum. & Meth. B,* **213**, 677-682 (2004).
10. D. H. Bilderback, *X-Spectrometry*, **32**, 195-207 (2003); Kumakhov, M. A., *X-ray Spectrom.*, **29**, 343-348 (2000).
11. K. Proost, K. Janssens, L. Vincze, G. Falkenberg, N. Gao, and P. Bly, Hasylab Annual report (2002); K.Janssens, K.Proost, G. Falkenberg, *Spectrochimica Acta,* 559,1637-164, (2004).
12. B. Kanngiesser, W. Malzer, I. Reiche, *Nucl. Inst. Meth. B*, **211**, 259 (2003).
13. G. J. Havrilla and Gao, N., *52nd Annual Denver X-ray Conference Abstracts*, **F28**, 120 (2004); Ding, X., Gao, N., and Havrilla, G. J., in *Advances in Laboratory-Based X-ray Sources and Optics*, MacDonald, C. and Khounsary, A. M. eds., *Proceedings of SPIE,* **4144**, 174-182 (2000).
14. R. Huang and D. H. Bilderback, 'Secondary Focusing for Micro-Diffraction Using One-Bounce Capillaries,' accepted for the Proceedings of Eighth International Conference on Synchrotron Radiation Instrumentation held August 25-29, 2003 in San Francisco; Huang, R. & D.H. Bilderback, *Nucl. Instrum. & Meth*. **A467**, 978-981 (2001).
15. C. Fiorini, A. Longoni, and A. Bjeoumikhov, *IEEE Trans. on Nuclear Science*, **48**(3), 268-271 (June 2001).
16. For additional information about XOS optics see http://www.xos.com.
17. The binder is a poly ethyl methacrylate / co-methacrylate copolymer blend from Rohm and Haas.
18. A. R. Woll, J. Mass, C. Bisculca, R. Huang, D. Bilderback, S. Gruner, and N. Gao 'Development of Confocal X-ray Fluorescence (XRF) Microscopy at the Cornell High Energy Synchrotron Source', (submitted).
19. Bockrath, M., copy from Diego Velasquez' "Prince Baltasar Carlos with a Dwarf," 1631 (MFA, Boston), 1997.
20. The higher order fluorescence energies of lead are taken from Bearden, J.A., *Rev. Mod. Phys.* **39**, 78 (1967).